Engineering xxx (xxxx) xxx

Contents lists available at ScienceDirect

Engineering

journal homepage: www.elsevier.com/locate/eng

Research
New Technology of Tumor Diagnosis and Treatment—Article

Targeted Therapy of Central Nervous System Acute Lymphoblastic Leukemia with an Integrin α6-Targeted Self-Assembling Proapoptotic Nanopeptide

Jia-Cong Ye [a,b,#], Wan-Qiong Li [c,1], Mei-Ling Chen [b,1], Qian-Kun Shi [d,1], Hua Wang [b], Xin-Ling Li [b], Ying-He Li [b], Jie Yang [b], Qiao-Li Wang [b], Fang Hu [d], Yan-Feng Gao [c,*], Shu-Wen Liu [a,e,*], Mu-Sheng Zeng [b,*], Guo-Kai Feng [b,*]

[a] Guangdong Provincial Key Laboratory of New Drug Screening & NMPA Key Laboratory of Drug Metabolism Research and Evaluation, School of Pharmaceutical Sciences, Southern Medical University, Guangzhou 510515, China
[b] State Key Laboratory of Oncology in South China & Guangdong Key Laboratory of Nasopharyngeal Carcinoma Diagnosis and Therapy, Guangdong Provincial Clinical Research Center for Cancer, Sun Yat-sen University Cancer Center, Guangzhou 510060, China
[c] School of Pharmaceutical Sciences (Shenzhen), Shenzhen Campus of Sun Yat-sen University, Shenzhen 518107, China
[d] Guangdong Provincial Key Laboratory of Construction and Detection in Tissue Engineering, Biomaterials Research Center, School of Biomedical Engineering, Southern Medical University, Guangzhou 510515, China
[e] State Key Laboratory of Organ Failure Research, Guangdong Provincial Institute of Nephrology, Southern Medical University, Guangzhou 510515, China

ARTICLE INFO

Article history:
Received 20 June 2023
Revised 7 November 2023
Accepted 8 November 2023

Keywords:
Central nervous system acute lymphoblastic leukemia
Integrin α6
Targeted peptide
Proapoptotic
Nanopeptide

ABSTRACT

There is currently no effective targeted therapeutic strategy for the treatment of central nervous system acute lymphoblastic leukemia (CNS-ALL). Integrin α6 is considered a potential target for CNS-ALL diagnosis and therapy because of its role in promoting CNS-ALL disease progression. The targeted peptide $_D$(RWYD) (abbreviated RD), with nanomolar affinity to integrin α6 was identified by peptide scanning techniques such as alanine scanning, truncation, and D-substitution. Herein, we developed a therapeutic nanoparticle based on the integrin α6-targeted peptide for treating CNS-ALL. The self-assembled proapoptotic nanopeptide $_D$(RWYD)-$_D$(KLAKLAK)$_2$-G$_D$(FFY) (abbreviated RD-KLA-Gffy) contains the integrin α6-targeted peptide RD, the well-known proapoptotic peptide $_D$(KLAKLAK)$_2$ (abbreviated KLA) and the self-assembling tetrapeptide G$_D$(FFY) (abbreviated Gffy). The functional mechanism of RD-KLA-Gffy is clarified using different experiments. Our results demonstrate that RD-KLA-Gffy is highly enriched in CNS-ALL lesions and induces tumor cell apoptosis, thus reducing CNS-ALL disease burden and prolonging the survival of CNS-ALL mice without obvious toxicity. Moreover, the combined use of RD-KLA-Gffy and methotrexate (MTX) shows a potent antitumor effect in treating CNS-ALL, indicating that RD-KLA-Gffy plays an important role in suppressing CNS-ALL progression either as a single agent or in combination with MTX, which shows promise for application in CNS-ALL therapy.

1. Introduction

In previous studies, it was reported that approximately 1%–5% of acute lymphoblastic leukemia (ALL) patients who were not undergoing central nervous system (CNS)-directed prophylaxis would relapse with CNS-ALL [1,2]. Currently, the main clinical treatment strategies for CNS leukemia are ① oral administration of glucocorticoids and dexamethasone, ② intravenous injection of high-dose methotrexate (MTX) combined with intrathecal injection, and ③ moderate radiotherapy [3–5]. Although these approaches achieved a clinically significant short-term effect, the neurotoxicity has a long-term effect on patients [6,7].

Antibody-based immunotherapy is a new method to improve CNS-ALL treatment. It has been reported that the use of chimeric antibodies against cluster of differentiation (CD) 19 and CD3, such as blinatumomab, effectively improves the clinical outcome

* Corresponding authors.
E-mail addresses: gaoyf29@mail.sysu.edu.cn (Y.-F. Gao), liusw@smu.edu.cn (S.-W. Liu), zengmsh@sysucc.org.cn (M.-S. Zeng), fengguok@sysucc.org.cn (G.-K. Feng).
# These authors contributed equally to this work.

https://doi.org/10.1016/j.eng.2023.11.012

Please cite this article as: J.-C. Ye, W.-Q. Li, M.-L. Chen et al., Targeted Therapy of Central Nervous System Acute Lymphoblastic Leukemia with an Integrin α6-Targeted Self-Assembling Proapoptotic Nanopeptide, Engineering, https://doi.org/10.1016/j.eng.2023.11.012

in patients positive for minimal residual disease (MRD). However, blinatumomab causes significant toxicity, resulting in CNS events and cytokine release syndrome [8,9]. Other antibodies, such as the CD19 monoclonal antibody CD19-DE [10], CD38 antibody daratumumab [11] and interleukin 7 receptor (IL7R) monoclonal antibody [12], have also achieved good therapeutic effects in preclinical animal models. The limitation of these antibody therapies, however, is their inefficient delivery to the CNS. Another novel strategy is chimeric antigen receptor T (CAR-T) cell immunotherapy. A clinical trial of CD19-CAR-T cell therapy showed that this regimen achieved good outcomes in chemotherapy-resistant childhood and adult ALL, with a reduced rate of cytokine release syndrome [12]. In another clinical trial on drug-resistant acute B-cell lymphoblastic leukemia (B-ALL), ALL cells were undetectable in the cerebrospinal fluid (CSF) of two CNS-ALL patients after CD19-CAR-T cell treatment [13]. In an international study of CAR-T cell therapy for relapsed B-ALL with CNS involvement, 51 of 54 evaluable patients (94%) achieved complete response, but relapse occurred in 22 of 54 patients (41%) [14]. Data from these clinical trials suggest that CAR-T therapy may be an effective treatment for CNS-ALL. However, existing clinical trials have used the different structure of CD19-CAR-T cell, resulting in inconsistent in efficacy, and the use of CAR-T cells is often accompanied by side effects such as cytokine release syndrome [15]. Therefore, safer and more effective CNS-targeted therapies are urgently needed.

Integrin α6 is a transmembrane protein encoded by the human integrin α6 gene (*ITGA6*) [16]. Naturally, integrin α6 interacts with β1 or β4 to form heterodimers, namely, integrins α6β1 and α6β4, which are abnormally overexpressed in a variety of tumors [17,18]. Integrins α6β1 and α6β4 are involved in the processes of tumor progression and immune escape, as well as the induction of tolerance to tumor chemotherapy and radiotherapy [17,19–24]. Analysis of the Gene Expression Profiling Interactive Analysis (GEPIA) cancer database[†] showed that the *ITGA6* gene was overexpressed in thirteen kinds of tumors, including acute myeloid leukemia (AML), which showed the highest tumor-to-normal tissue ratio of 360.75 among them (Table S1 in Appendix A). In a clinical study of relapsed AML, the expression of integrin α6 was significantly upregulated, suggesting that integrin α6 may act as an important therapeutic target for refractory AML [21]. Furthermore, integrin α6 has been reported to be overexpressed in B-ALL, and the deletion of integrin α6 induced apoptosis in B-ALL cells [25]. Moreover, integrin α6 has been demonstrated to interact with laminin to induce the migration of ALL cells into CSF, suggesting that integrin α6 expression directly promotes CNS-ALL disease progression [26]. Another study confirmed that phosphoinositide 3-kinase (PI3K) inhibitors can reduce the expression of integrin α6, thus decreasing CNS involvement and prolonging the survival of B-ALL mice [26]. Additionally, integrin α6 has been demonstrated to mediate B-ALL drug resistance [21,25]. In summary, integrin α6 plays an important role in the migration of ALL cells toward the CNS, as well as in B-ALL drug resistance.

Previously, we identified an integrin α6-targeted peptide, CRWYDENAC (abbreviated RWY), by using phage display and next-generation sequencing techniques [27]. Similar to the integrin αvβ3-targeting peptide arginine-glycine-asparticacid (RGD), the identified peptide RWY shows high-affinity to tumors through binding to integrin α6. The RWY peptide has been employed for molecular imaging and targeted therapy in several kinds of tumors, including nasopharyngeal carcinoma [27], hepatocellular carcinoma (HCC) [28] and intestinal carcinoma [29] in mouse models and breast cancer in patients [30]. Recently, we performed alanine scanning of the integrin α6-targeted peptide RWY and identified three key amino acids, namely, arginine (R), tryptophan (W), and tyrosine (Y), which mediated the peptide's tumor-targeting ability [31]. Moreover, we constructed an optimized integrin α6-targeted peptide, CRWYDANAC (abbreviated S5), which showed a twofold improvement in binding affinity to integrin α6 compared with the RWY peptide [31]. Based on peptide S5, three molecular imaging probes, cyanine 5 (Cy5)-S5 for near-infrared fluorescence (NIRF), gadolinium (Gd)-S5 for magnetic resonance (MR), and ^{18}F-S5 for positron emission tomography (PET) imaging, were developed and employed for CNS-ALL imaging [32]. These previous studies demonstrated that integrin α6-targeted peptides are ideal vehicles to deliver imaging or treatment agents for CNS-ALL diagnosis and therapy.

In this study, we identified an optimized integrin α6-targeted peptide with nanomolar affinity to integrins α6β1 and α6β4 using peptide scanning techniques. Based on this peptide, we developed an integrin α6-targeted self-assembling nanopeptide $_D$(RWYD)-$_D$(KLAKLAK)$_2$-G$_D$(FFY) (abbreviated RD-KLA-Gffy), which consists of the newly identified integrin α6-targeted peptide $_D$(RWYD) (abbreviated RD), the proapoptotic peptide $_D$(KLAKLAK)$_2$ (abbreviated KLA) [33] and the self-assembling peptide G$_D$(FFY) (abbreviated Gffy) [34]. RD-KLA-Gffy induced apoptosis of leukemia cells *in vitro* and *in vivo*, and thus showed an antileukemia effect when used as a single agent or combined with MTX, a traditional chemotherapeutic drug for ALL therapy.

2. Materials and methods

2.1. Cell culture

HCC cell lines, including HCC-LM3, Huh7 and Hep3B; leukemia cell lines, including Nalm6, Jurkat and K562; and the ovarian cancer cell line HeLa, were purchased from the American Type Culture Collection (ATCC) (USA). HCC-LM3, Huh7, Hep3B, and HeLa cells were cultured in DMEM; and Nalm6, Jurkat, and K562 cells were cultured in RPMI 1640 medium supplemented with 10% fetal bovine serum and 0.5% penicillin–streptomycin. To further verify the binding affinities of the peptides to cells, HCC-LM3 and HeLa cells were stably transfected with *ITGA6* knockout lentivirus using the clustered regularly interspaced short palindromic repeats/CRISPR-associated protein 9 (CRISPR/Cas9) genome editing system (OBiO Technology, China). To facilitate tumor monitoring, Nalm6 cells were stably transfected with luciferase (OBiO Technology). All cells were regularly authenticated and confirmed to be mycoplasma-negative.

2.2. Synthesis of peptide

All peptides involved in this study were synthesized by the China Peptide Company (China), which provided complete quality control reports. The amino acid sequences of all peptides involved in this study are as follows: cyclic peptides CRWYDENAC (abbreviated RWY), CAWYDENAC, CRAYDENAC, CRWADENAC, CRWYAENAC (abbreviated M4), CRWYDANAC (abbreviated S5), CRWYDEAAC (abbreviated M5), RWYDENA, RWYDANA, RWYDEN, RWYDAN, RWYDE, and RWYDA; linear peptides RWYD, RWY, and $_D$(RWYD) (abbreviated RD); fluorescent peptides CRWYDENAC-PEG4-K-FITC (abbreviated FITC-RWY) and RWYD-PEG4-K-FITC (abbreviated FITC-RWYD); nanopeptides and control peptides $_D$(RWYD)-$_D$(KLAKLAK)$_2$-G$_D$(FFY) (abbreviated RD-KLA-Gffy), $_D$(CRWYAENAC)-$_D$(KLAKLAK)$_2$-G$_D$(FFY) (abbreviated M4-KLA-Gffy), $_D$(CRWYDEAAC)-$_D$(KLAKLAK)$_2$-G$_D$(FFY) (abbreviated M5-KLA-Gffy), $_D$(CRWYDENAC)-$_D$(KLAKLAK)$_2$-G$_D$(FFY) (abbreviated RWY-KLA-Gffy), $_D$(KLAKLAK)$_2$-G$_D$(FFY) (abbreviated KLA-Gffy), $_D$-

[†] www.gepia.cancer-pku.cn.

(RWYD)-$_D$(KLAKLAK)$_2$ (abbreviated RD-KLA), $_D$(KLAKLAK)$_2$ (abbreviated KLA), and $_D$(RWYD)-G$_D$(FFY) (abbreviated RD-Gffy).

2.3. Microscale thermophoresis (MST) assay

In the MST assay, fluorescence labeling of integrin α6β4 or α6β1 recombinant protein (#CT069-H2508H or #CT013-H2508H, Sino Biological, China) was performed with the reactive dye RED-tris-NTA (#MO-L018, NanoTemper Technologies, Germany), which reacts with the primary amines of a protein to form a stable dye-protein conjugate. Analytes with different concentrations of peptides (Chinese Peptide Company, China) were incubated with labeled protein for 5 min at 25 °C, and then the mixtures in the tubes were absorbed into capillaries (#MO-K022, NanoTemper Technologies) for sample detection by Monolith NT.115 (NanoTemper Technologies) and final analysis.

2.4. Molecular docking

The crystal structure of integrin α6 was obtained by SWISS-MODEL homology modelling [35], and optimized by adding exclusive hydrogens and missing atoms. The three-dimensional structure of the peptide was created by the PEPstrMOD server [36,37], and unbiased docking to the optimal structure of integrin α6 was performed by using the ZDOCK server [38]. Molecular operating environment (MOE) software was used to analyze the docking mode between the protein and peptide, and the best docking mode was selected by combining the indices of binding force and interaction site [39].

2.5. Flow cytometry

To detect the expression of integrin α6 in cells, cells were seeded at a density of 1×10^6 cells per milliliter in 6-well plates and then stained with 10 μL per 1×10^6 cells integrin α6 antibody (vFAB13501P, R&D Systems, USA) and immunoglobulin G2A (IgG2A) antibody (#IC006P, R&D Systems) at 4 °C. After incubation for 30 min, the cells were washed three times with phosphate buffered saline (PBS) and analyzed on a CytoFLEX S cytometer (Beckman Coulter, USA). To investigate the binding of peptide RD to cells, cells were seeded at a density of 1×10^6 cells per milliliter in a 6-well plate and then stained with 1 μmol·L^{-1} FITC-peptide (Chinese Peptide Company, China) at 37 °C. After incubation for 60 min, the cells were washed three times with PBS and analyzed on a CytoFLEX S cytometer. To verify the principle by which the nanopeptide kills leukemia cells, cells were seeded at a density of 1×10^6 cells per milliliter in 6-well plates and then incubated with 5 μmol L^{-1} peptides at 37 °C. After incubation for 60 min, the cells were washed three times with PBS and stained with Annexin V/PI (#BMS500FI, Invitrogen, USA) at 4 °C. After incubation for 30 min, the cells were washed three times with PBS and analyzed on a CytoFLEX S cytometer.

2.6. Physical characterization of the nanopeptides

The nanopeptides were synthesized and analyzed by high-performance liquid chromatography (HPLC) and mass spectrometry (MS) by the Chinese Peptide Company. The critical aggregation concentration (CAC) values were determined by dynamic light scattering (DLS) (Malvern, UK). Solutions containing different concentrations of compounds were tested, and the light scattering intensities were recorded for final analysis. The zeta potentials and sizes of the nanopeptides were determined by DLS. Transmission electron microscopy (TEM) images of the nanopeptides were acquired with a TEM microscope (FEI Tecnai Spirit TEM T12, USA) at 100 000-fold magnification.

2.7. Cytotoxicity of the nanopeptides

To determine the cytotoxicity of the nanopeptides, cells were seeded at a density of 1×10^6 cells per milliliter in a 96-well plate and then incubated with different concentrations of peptides (Chinese Peptide Company) at 37 °C. After incubation for 3 h, the cells were stained with cell counting kit-8 (CCK-8) (#C0039, Beyotime, China). Three hours later, the cells were analyzed by ultraviolet (UV) spectroscopy (BioTek Synergy H1, USA). To monitor the cytotoxicity of the peptides to cells in real time, cells were seeded at a density of 5×10^4 cells per milliliter in a 96-well plate. Then, the cells were incubated with 5 μmol·L^{-1} peptides accompanied by 2.5 μmol·L^{-1} SYTOX Green nucleic acid stain (#S7020, Invitrogen) and photographed every 10 min using a cell real-time monitoring system (Essen Bioscience IncuCyte S3, USA).

2.8. Protein extraction and western blotting

After incubation with 5 μmol·L^{-1} peptides for 3 h, the cells were washed with PBS. Proteins were extracted and dissolved in RIPA lysis buffer (#P0013B, Beyotime). Protein concentrations were determined by the Bradford assay (#23225, Thermo Fisher, USA). The proteins were separated by sodium dodecyl sulfate polyacrylamide gel electrophoresis (SDS-PAGE) and transferred to polyvinylidene fluoride (PVDF) membranes, which were then incubated with antibodies overnight at 4 °C, including anti-caspase-3 (1 : 2000, #ab32351, Abcam, UK), anti-cleaved caspase-3 (1 : 500, #ab32042, Abcam), anti-caspase-8 (1 : 2000, #ab227430, Abcam), anti-poly(ADP-ribose) polymerase-1 (PARP1) (1 : 1000, #ab191217, Abcam), anti-cleaved PARP1 (1 : 1000, #ab32064, Abcam), anti-B cell lymphoma-2 (BCL-2) (1 : 1000, #15071, Cell Signaling Technology, USA), and anti-β-tubulin (1 : 1000, #2146, Cell Signaling Technology). Finally, goat anti-rabbit horseradish peroxidase-labeled immunoglobulin G (IgG-HRP) antibody (1 : 10 000, #G-21234, Thermo Fisher) and goat anti-mouse IgG HRP antibody (1 : 10 000, #31430, Thermo Fisher) were used as secondary antibodies.

2.9. Mouse engraftment

The mouse experiments were approved by the Institutional Animal Care and Use Committee (IACUC) of Sun Yat-sen University Cancer Center (IACUC approval number L025501202204008). To generate xenograft mice, 6-week-old female BALB/c-nude mice (Shanghai Model Organisms Center, China) were inoculated subcutaneously with 1×10^6 Nalm6-luciferase-enhanced green fluorescent protein (luc-EGFP) cells. Similarly, to generate CNS-ALL mice [26], 6-week-old female NOD/SCID/IL-2Rγ (NSG) mice (Shanghai Model Organisms Center, China) were inoculated intravenously with 1×10^6 Nalm6-luc-EGFP cells. When Nalm6-luc-EGFP cells could be observed in the head (meninge) by luminescence imaging approximately eight days later, the CNS-ALL mouse model was considered to have been successfully constructed.

2.10. NIRF imaging

To verify the tumor accumulation of the nanopeptide, RD-KLA-Gffy was labeled to display red fluorescence with an EZLabel protein Cy5 labeling kit (#K839-5, BioVision, USA), and high-purity Cy5-labeled RD-KLA-Gffy (abbreviated Cy5-RD-KLA-Gffy) and Cy5-labeled KLA-Gffy (abbreviated Cy5-KLA-Gffy) were obtained by molecular sieving (General Electric, USA). NIRF imaging was performed using an in vivo imaging system (IVIS) spectrum (PerkinElmer, USA) at 1, 12, 24, and 48 h after 0.5 mg·kg^{-1} Cy5-RD-KLA-Gffy was injected intravenously into subcutaneous xenograft mice or CNS-ALL mice. Luminescence imaging was performed starting

5 min after intraperitoneal injection of 150 mg kg^{-1} luciferin (#P1041, Promega, USA), and NIRF images were acquired with excitation at 640 nm and emission at 680 nm. After NIRF imaging, the mice were euthanized by cervical dislocation and immediately dissected. Luminescence and NIRF signals from the tumor and vital organs were recorded.

2.11. Immunofluorescence, hematoxylin and eosin (HE) staining and immunohistochemistry (IHC)

The brains of the CNS-ALL mice were cut into frozen sections, stained with 1 μg·mL^{-1} 4',6-diamidino-2-phenylindole (DAPI) (#28718-90-3, Sigma, USA) and mounted on slides with ProLong Gold Antifade (P26930, Invitrogen). Fluorescence images were captured under a confocal microscopy confocal laser scanning system (3DHISTECH Pannoramic MIDI, Hungary). In the fluorescence images, blue fluorescence represents the nucleus, green fluorescence represents Nalm6-luc-EGFP cells, and red fluorescence represents the nanopeptide Cy5-RD-KLA-Gffy. The frozen sections were also stained with HE according to routine histological procedures. Furthermore, frozen sections were used for IHC with an anti-integrin α6 antibody (1 : 150, #ab181551, Abcam). IHC was performed following the conventional procedure we reported previously [28], and images were observed under a microscope (Nikon Eclipse, Japan).

2.12. Survival experiment

As described for the mouse engraftment experiment, when the CNS-ALL mouse model was successfully constructed, the mice were divided into groups with 10 mice per group. The mice were intravenously treated with drugs every two days. The concentration of RD-KLA-Gffy and control peptides was 5 mg·kg^{-1}. The concentration of MTX was 2 mg·kg^{-1}. The body weights and survival curves of the CNS-ALL mice were monitored. Nalm6-luc-EGFP cell metastasis was detected by luminescence imaging.

2.13. Statistical analysis

All statistical analyses were performed using GraphPad Prism software (Version 8.3.0.538). Statistical evaluations were performed using either one-way analysis of variance (ANOVA) or two-way ANOVA, and the results are shown as the mean ± standard deviation (SD). Statistical analyses of the survival experiments were performed using log-rank tests. P values are denoted as follows: no significance (ns), $P > 0.05$; $^{*}P < 0.05$; $^{**}P < 0.01$; and $^{***}P < 0.001$.

3. Results

3.1. Identification of the high-affinity integrin α6-targeted peptide

Although the integrin α6-targeted peptides RWY and S5 can both be highly enriched in tumor tissues [27,28,31], their binding affinities to integrins α6β1 and α6β4 are still relatively low (micromolar range). To obtain optimized integrin α6-targeted peptides with improved binding affinity to integrins α6β1 and α6β4, three peptide scanning techniques, namely, alanine scanning, truncation, and D-substitution, were performed (Fig. 1(a)). Beginning with the previously identified integrin α6-targeted peptides RWY and S5, we designed and synthesized a series of mutant peptides by using alanine scanning and truncation techniques. Then, we determined the binding affinity of the candidate peptides to integrin α6β4 by using MST analysis, and the dissociation constants (K_d values) of RWY and S5 were (6.97 ± 1.44) μmol·L^{-1} and (4.34 ± 3.42) μmol·L^{-1}, respectively (Table 1). Among these mutant peptides, the linear mutant peptide RWYD demonstrated the highest binding affinity (K_d = (21.82 ± 3.86) nmol·L^{-1}), which was approximately 319-fold more potent than that of the peptide RWY (Fig. 1(b)). Moreover, two cyclic mutant peptides, M4 and M5, also showed significantly improved affinities with enhancements of 17- and 11-fold, respectively (Table 1; Fig. S1 in Appendix A), compared to RWY. Additionally, the binding affinity of the linear peptide RWYD to integrin α6β1 was (23.95 ± 6.10) nmol·L^{-1}, which was approximately 235-fold more potent than that of the peptide RWY (K_d = (5.63 ± 1.01) μmol·L^{-1}) (Fig. 1(b)). In summary, these results demonstrate that the linear peptide RWYD is an ideal integrin α6-targeted peptide with nanomolar binding affinities to integrin α6β4 (K_d = (21.82 ± 3.86) nmol·L^{-1}) and integrin α6β1 (K_d = (23.95 ± 6.10) nmol·L^{-1}).

Furthermore, to determine the key amino acids that mediate the binding of the peptide RWYD to integrin α6, molecular docking analysis was performed. The interaction sites of the RWYD and RWY peptides on integrin α6 are highlighted (Fig. 1(c)). RWYD formed three hydrogen bonds (R1-S331, Y3-Y450, and D4-H110) and one aromatic hydrophobic interaction (W2-Y273). In comparison, the previously identified peptide RWY formed two hydrogen bonds (R2-S331 and Y4-R111) and one aromatic hydrophobic interaction (W3-F23). Compared to peptide RWY, RWYD showed one more binding interaction (D4-H110), which may explain why the binding affinity of peptide RWYD to integrins α6β4 and α6β1 is stronger than that of peptide RWY.

3.2. Binding specificity of the optimized integrin α6-targeted peptide

To determine whether the integrin α6 expression level plays an important role in affecting the affinity of the optimized integrin α6-targeted peptide RWYD correlates, two FITC-labeled peptides, FITC-RWY and FITC-RWYD, were synthesized, and their affinity to three HCC cell lines with different expression levels of integrin α6 was examined. The expression levels of integrin α6 were first determined using an α6 antibody, and the data showed that the expression of integrin α6 was high in HCC-LM3 cells, moderate in Huh7 cells, and low in Hep3B cells (Fig. 2(a)). In line with the different expression levels of integrin α6, the cell binding ability of the peptide FITC-RWYD was high in HCC-LM3 cells, moderate in Huh7 cells and low in Hep3B cells (Figs. 2(b), (c) and (d)). Comparatively, in cell lines with high and moderate expression of integrin α6 (HCC-LM3 and Huh7), the cell binding ability of FITC-RWYD was significantly higher than that of peptide FITC-RWY (Fig. 2(e)). However, in Hep3B cells with low integrin α6 expression, there was no significant difference between the cell binding abilities of peptides FITC-RWYD and FITC-RWY (Fig. 2(e)). Additionally, we explored the cell binding abilities of FITC-RWYD to three leukemia cell lines, including Nalm6, Jurkat and K562. Similar to HCC cells, FITC-RWYD bound more strongly than FITC-RWY to Nalm6 and Jurkat cells, which exhibit high expression of integrin α6. Moreover, there was no significant difference between the peptides FITC-RWYD and FITC-RWY in cell affinity to K562 cells, which have low integrin α6 expression (Fig. S2 in Appendix A). These results demonstrated that the cell binding ability of the optimized integrin α6-targeted peptide RWYD is correlated with the expression level of integrin α6.

To further determine the binding specificity of the peptide RWYD, the CRISPR/Cas9 genome editing system was used to knock out (KO) the *ITGA6* in the HCC cell line HCC-LM3 and the ovarian cancer cell line HeLa, both of which exhibit high expression of integrin α6 (Fig. 2(f)). As expected, in *ITGA6* knockout HCC-LM3-KOα6 and HeLa-KOα6 cells, the cell binding ability of the peptide FITC-RWYD was completely abolished (Figs. 2(g), (h) and (i)). These results clarified that the cell binding ability of the optimized inte-

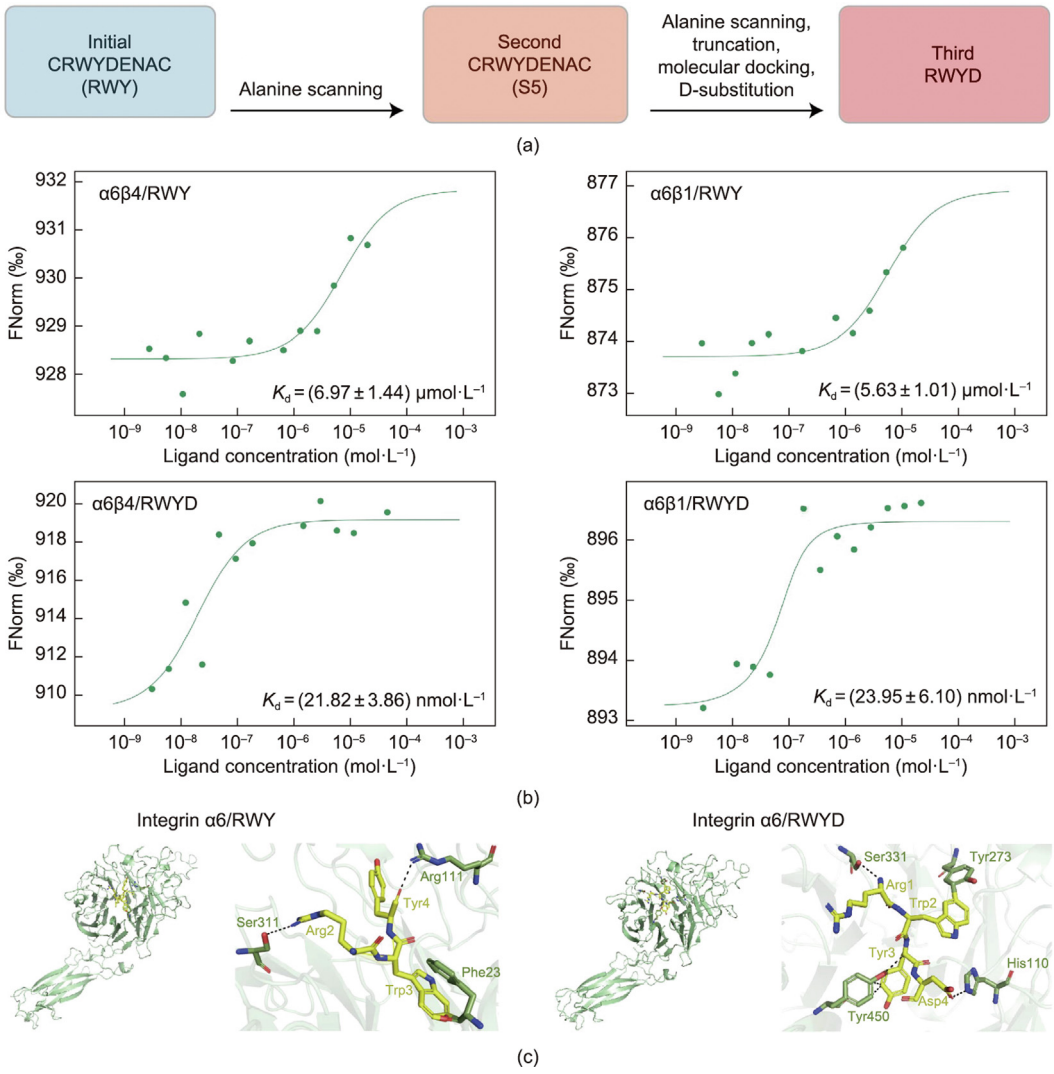

Fig. 1. Identification of the high-affinity integrin α6-targeted peptide RWYD. (a) Schematic illustration of the optimization of the integrin α6-targeted peptide. (b) The binding affinities of the peptides to integrin α6β4. RWY and the mutated peptide RWYD were synthesized, and their binding affinities to integrins α6β4 and α6β1 were measured by MST assay. Data are presented as the mean ± SD, n = 3. (c) The binding mode of RWY and RWYD to integrin α6 was simulated by molecular docking. In the overall docking pose, the integrin α6 is shown in green, RWY and RWYD are shown in yellow, and the interaction area between integrin α6 and RWY/RWYD is highlighted. Ser331: Serine321; Arg2: Arginine2; Trp3: Tryptophan3; Phe23: Phenylalanine23; Tyr4: Tyrosine4; Arg111: Arginine111; Arg1: Arginine1; Trp2: Tryptophan2; Tyr273: Tyrosine273; Tyr3: Tyrosine3; Tyr450: Tyrosine450; Asp4: Asparticacid4; His110: Histidine110.

Table 1
Binding affinities of the mutant peptides to integrin α6β4. Binding affinities were measured by MST assay. Data are presented as the mean and SD, n = 3.

Sequences	Cyclic/linear	K_d (μmol·L^{-1})			Mean	SD	Relative to RWY
		1	2	3			
RWY	Cyclic	8.59	6.52	5.81	6.97	1.44	1.00
CAWYDENAC	Cyclic	4.03	12.13	3.58	6.58	4.81	1.06
CRAYDENAC	Cyclic	14.40	11.76	13.85	13.34	1.39	0.52
CRWADENAC	Cyclic	–	–	–	–	–	–
M4	Cyclic	0.36	0.22	0.65	0.41	0.22	17.01
S5	Cyclic	1.21	7.99	3.83	4.34	3.42	1.61
M5	Cyclic	0.25	0.25	1.37	0.62	0.65	11.19
RWYDENA	Cyclic	–	–	–	–	–	–
RWYDANA	Cyclic	62.05	17.53	12.38	30.65	27.31	0.23
RWYDEN	Cyclic	9.69	8.73	13.09	10.50	2.29	0.66
RWYDAN	Cyclic	34.65	23.19	35.69	31.18	6.94	0.22
RWYDE	Cyclic	14.73	78.75	99.63	64.37	44.24	0.11
RWYDA	Cyclic	6.28	4.69	4.22	5.06	1.08	1.38
RWYD	Linear	0.02	0.02	0.02	0.02	0	319.43
RWY	Linear	–	–	–	–	–	–

Three mutant peptides, CRWADENAC, RWYDENA and RWY, did not bind to integrin α6β4.

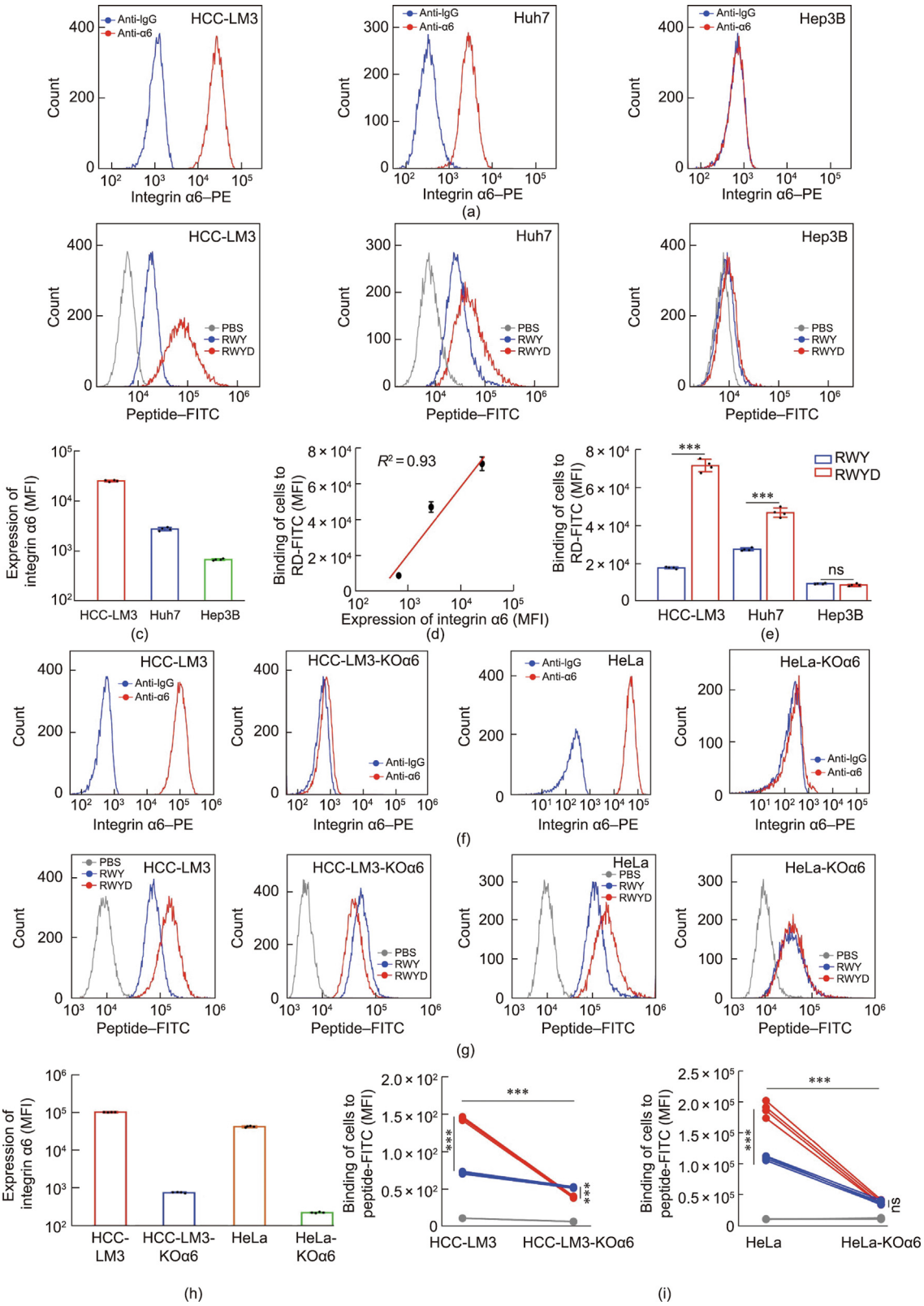

Fig. 2. Binding specificity of the integrin α6-targeted peptide RWYD. (a) Flow cytometry was used to determine the surface expression of integrin α6 in human HCC cell lines, including HCC-LM3, Huh7, and Hep3B. (b) Flow cytometry was used to determine the binding between FITC-RWY/FITC-RWYD and HCC cells. (c) Quantitative analysis of the fluorescence intensity was used to evaluate the surface expression of integrin α6 in HCC cell lines. (d) Quantitative analysis of the fluorescence intensity of FITC-RWYD bound to HCC cells. (e) The expression of integrin α6 in cells was positively correlated with the binding ability of FITC-RWYD. (f) Flow cytometry was used to determine the surface expression of integrin α6 in *ITGA6* knockout and wild-type cells. (g) Flow cytometry determined the binding affinity of FITC-RWY/FITC-RWYD to *ITGA6* knockout and wild-type cells. (h) Quantitative analysis of the fluorescence intensity was used to evaluate the surface expression of integrin α6 in *ITGA6* knockout and wild-type cells. (i) Quantitative analysis of the fluorescence intensity of FITC-RWY/FITC-RWYD bound to *ITGA6* knockout and wild-type cells. Significance was determined by one-way ANOVA, $n = 4$, $^{***}P < 0.001$. α6: integrin α6; PE: phycoerythrin; FITC: fluorescein isothiocyanate; MFI: median fluorescence intensity; KOα6: knock out *ITGA6*.

grin α6-targeted peptide RWYD mainly depended on the expression of integrin α6.

3.3. Characteristics of integrin α6-targeted self-assembling nanopeptide RD-KLA-Gffy

Considering that right-handed amino acids are usually more stable than left-handed amino acids *in vivo*, the D-substitution technique was performed. The MST results showed that the binding affinities of the right-handed peptide RD to integrin α6β4 (K_d = (30.29 ± 2.83) nmol·L^{-1}) and α6β1 (K_d = (19.23 ± 3.04) nmol·L^{-1}) were similar to those of the left-handed peptide RWYD to integrins α6β4 (K_d = (21.82 ± 3.86) nmol·L^{-1} and α6β1 (K_d = (23.95 ± 6.10) nmol L^{-1}) (Table 2; Fig. S3 in Appendix A). Therefore, the right-handed integrin α6-targeted peptide RD was used in the following study.

Previously, based on integrin α6-targeted peptide S5, three integrin α6-targeted peptide-based molecular probes were developed and employed for the accurate detection of CNS-ALL in a mouse model using different imaging strategies, such as Cy5-S5 for NIRF, Gd-S5 for MR imaging, and ^{18}F-S5 for PET imaging [32]. These integrin α6-targeted probes were highly enriched in CNS-ALL lesions in the mouse models, suggesting that the use of integrin α6-targeted peptides is valuable for CNS-ALL targeting. Therefore, an integrin α6-targeted self-assembling nanopeptide RD-KLA-Gffy consisting of an integrin α6-targeted peptide RD, a proapoptotic peptide KLA [33] and a self-assembling tetrapeptide Gffy [34] was designed (Fig. 3(a)). Among the different elements of RD-KLA-Gffy, integrin α6 and the tumor-targeting peptide RD mediated tumor enrichment, the proapoptotic peptide KLA induced tumor cell apoptosis, and the backbone of the nanopeptide Gffy facilitated self-assembly into RD-KLA-Gffy nanoparticles. The synthesis process of the nanopeptide RD-KLA-Gffy is shown in Fig. S4 in Appendix A. The nanopeptide was purified and identified using HPLC chromatogram and MS spectrum (Fig. S5 in Appendix A). The basic nanocharacteristics of RD-KLA-Gffy were examined by DLS. The CAC value of RD-KLA-Gffy was 2.52 μmol·L^{-1} (Fig. 3(b)), and its zeta potential was 7.07 mV (Fig. 3(c)), which indicates a high tendency to assemble. Its hydrodynamic diameter was 21.8 nm (Fig. 3(d)), as measured by DLS, similar to the data detected by TEM images (Fig. 3(e)). Moreover, the affinities of RD-KLA-Gffy for integrins α6β4 and α6β1 were (70.6 ± 3.4) nmol·L^{-1} and (25.7 ± 4.3) nmol·L^{-1}, respectively, which were slightly lower than those of the single peptide RD (K_d = (30.29 ± 2.83) nmol·L^{-1} for integrin α6β4 and K_d = (19.23 ± 3.04) nmol·L^{-1} for integrin α6β1) (Fig. 3(f)).

3.4. Antitumor effect of the integrin α6-targeted self-assembling nanopeptide RD-KLA-Gffy

In addition to RD-KLA-Gffy, we synthesized other nanopeptides: M4-KLA-Gffy, M5-KLA-Gffy, and RWY-KLA-Gffy, as controls (Fig. S6(a) in Appendix A). To determine their antitumor effects, cell viability assays were performed using CCK-8. The data showed that all nanopeptides had dose-dependent cytotoxicity, among which RD-KLA-Gffy was the most toxic to Nalm6 cells, with a half maximal inhibitory concentration (IC_{50}) value of 3.15 μmol·L^{-1} (Fig. S6(b) in Appendix A). Then, we incubated Nalm6 cells with RD-KLA-Gffy and the peptide controls at a concentration of 5 μmol·L^{-1}, along with SYTOX green nucleic acid staining, and photographed the cells every ten minutes. The results showed that RD-KLA-Gffy had the greatest toxicity, with a significant difference from the control, over the first forty minutes (Figs. S6(c) and (d) in Appendix A).

We also detected the toxicity of these nanopeptides in other tumor cells that highly express integrin α6, such as leukemia cell Jurkat, nasopharyngeal carcinoma cells HNE1 and S18, esophageal carcinoma cells KYSE30 and KYSE450, colorectal carcinoma cell SW620, and cervical carcinoma cell HeLa (Fig. S7(a) in Appendix A). The results showed that the IC_{50} values of RD-KLA-Gffy in these tumor cells were less than 10 μmol·L^{-1}, while many IC_{50} values of M4-KLA-Gffy, M5-KLA-Gffy, and RWY-KLA-Gffy were higher than 10 μmol·L^{-1}, indicating that the cytotoxicity of these nanopeptides to tumor cells was positively correlated with the binding ability of the targeting peptides (Fig. S7(b) and Table S2 in Appendix A).

Then, we constructed several peptide controls, such as KLA-Gffy, RD-KLA, KLA, and RD-Gffy (Fig. 4(a)), and determined their toxicity in Nalm6 cells. The data showed that the IC_{50} of RD-KLA-Gffy was the lowest (5.12 μmol·L^{-1}), which was approximately one-third that of KLA-Gffy (14.17 μmol·L^{-1}) and one-quarter that of RD-KLA (22.09 μmol·L^{-1}) (Fig. 4(b)), indicating that RD-KLA-Gffy possessed the strongest cytotoxicity. Moreover, after treatment for 150 min, the percentage of SYTOX-positive Nalm6 cells was 2.39% in the PBS control group, 9.09% in the KLA control group, 2.54% in the RD-Gffy control group, 25.50% in the RD-KLA control group, and 54.61% in the KLA-Gffy control group, while in the RD-KLA-Gffy group, approximately 91.78% of cells were positive (Figs. 4(c) and (d)). In Jurkat cells, RD-KLA-Gffy also showed fast and potent cytotoxicity (Fig. S8(a) and (b) in Appendix A).

After verifying the cytotoxicity of RD-KLA-Gffy in ALL cells, we explored the mechanism underlying the killing process. Considering that the nanopeptide contains the proapoptotic peptide KLA, we measured apoptotic markers using annexin V/propidium iodide (annexin V/PI) staining and flow cytometry analysis, as well as western blotting assays. Flow cytometry analysis showed that 98.88% of the Nalm6 cells exhibited spreading characteristic of late-stage apoptosis after 3 h of RD-KLA-Gffy treatment. In addition, 89.23% of KLA-Gffy-treated cells and 61.58% of RD-KLA-treated cells underwent apoptosis, but the cell status in the RD-Gffy, KLA, and PBS control groups remained nearly unchanged (Fig. 4(e)). In addition, RD-KLA-Gffy induced apoptosis in 99.98% of Jurkat cells (Fig. S8(c) in Appendix A). Subsequently, we examined the changes in the expression of several main apoptotic proteins by western blotting and found that the expression of caspase-3, caspase-8, PARP, and BCL-2 was downregulated, while the expression of cleaved caspase-3 and cleaved PARP was upregulated (Fig. 4(f)). Taken together, these results suggest that the leukemia cytotoxicity of the nanopeptide RD-KLA-Gffy was mainly induced by a proapoptotic effect.

3.5. The tumor-targeting ability of the integrin α6-targeted self-assembling nanopeptide RD-KLA-Gffy

To verify the antileukemic effect of the RD-KLA-Gffy nanopeptide *in vivo*, we labeled the nanopeptide with Cy5 fluorescence using a Cy5-labeling kit and purified it using molecular sieving (Fig. S9 in Appendix A). Then, Cy5-RD-KLA-Gffy was injected into Nalm6-luc-EGFP tumor-bearing mice through the tail vein. Forty-eight hours later, Cy5-RD-KLA-Gffy was significantly enriched in the tumor, while the uptake in the skin or metabolic organs, such as the intestine, kidney, and bladder, was low (Fig. S10(a) in Appendix A). Moreover, the red fluorescence of Cy5-RD-KLA-Gffy and luminescence of Nalm6-luc-EGFP cells showed strong colocalization in the subcutaneous tumors. Subsequently, the mice were euthanized, and the main organs and tumors were collected and analyzed. The data also showed that Cy5-RD-KLA-Gffy was mainly distributed in tumor tissues and colocalized with luminescent Nalm6-luc-EGFP cells (Fig. 5(a); Fig. S10(b) in Appendix A). In addition, the distribution of Nalm6-luc-EGFP cells in the head and spine of CNS-ALL mice bearing Nalm6-luc-EGFP (Fig. S11 in Appendix A) was observed by luminescence, and these cells colocalized with Cy5-RD-KLA-Gffy, indicating that Cy5-RD-KLA-Gffy could specifically target CNS-ALL (Fig. 5(b)). In addition, Cy5-KLA-Gffy showed slight colocalization with Nalm6-luc-EGFP cells (Fig. S12 in Appen-

Table 2
The binding affinities of the peptides to integrins α6β4 and α6β1. Binding affinities were measured by MST assay. Data are presented as the mean and SD, n = 3.

Sequence	Integrin α6β4 (nmol·L^{-1})					Integrin α6β1 (nmol·L^{-1})				
	1	2	3	Mean	SD	1	2	3	Mean	SD
RD	32.26	27.05	31.56	30.29	2.83	22.64	16.82	18.24	19.23	3.04

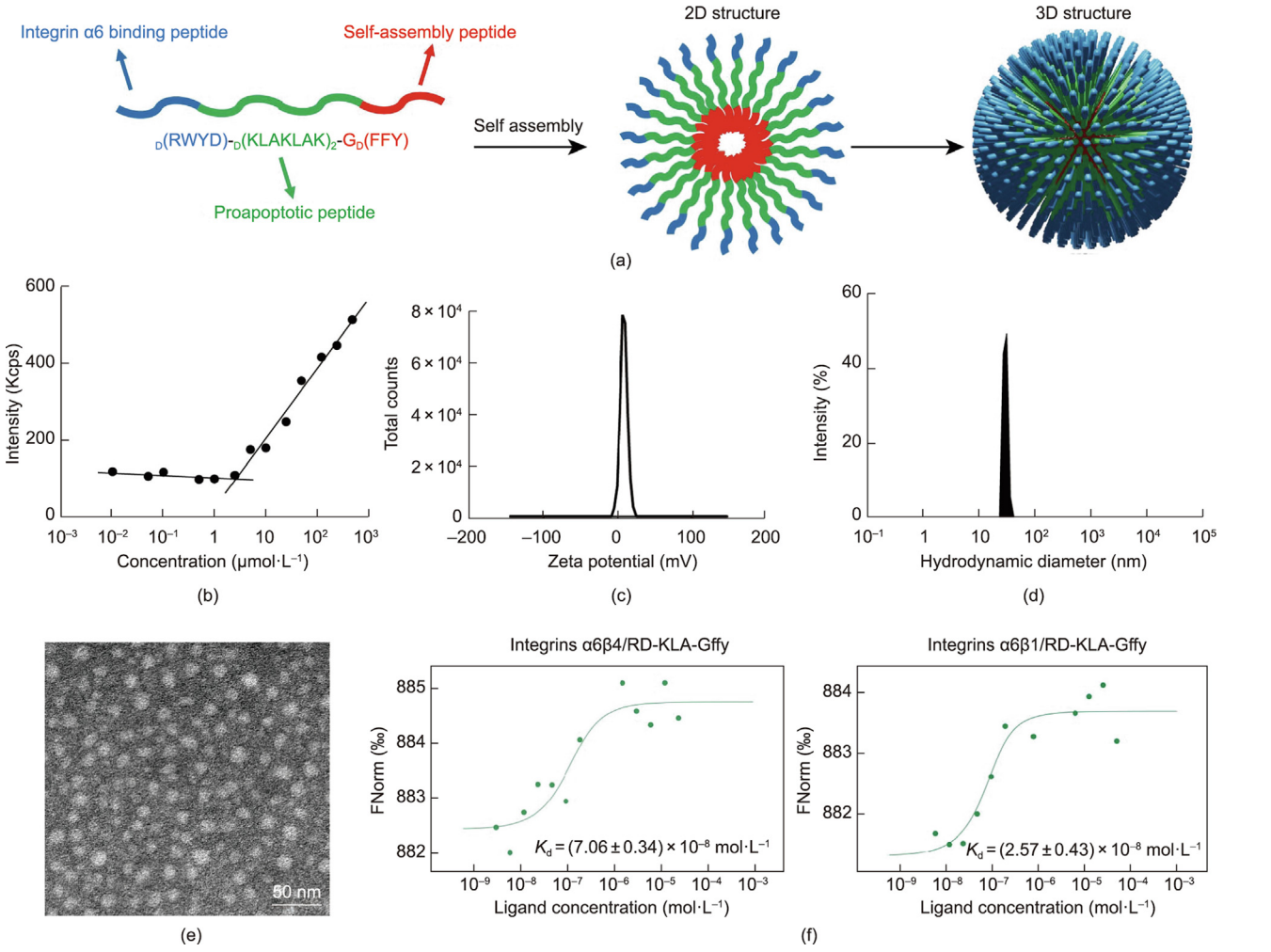

Fig. 3. Characteristics of the integrin α6-targeted self-assembling nanopeptide RD-KLA-Gffy. (a) Structural illustration and schematic diagram of the self-assembly of RD-KLA-Gffy. The (b) CAC value, (c) zeta potential, and (d) size of RD-KLA-Gffy were determined by DLS analysis. (e) Representative TEM images of RD-KLA-Gffy. (f) The binding affinities of RD-KLA-Gffy to integrins α6β4/α6β1 were determined by the MST assay. 2D: two-dimensional; Kcps: 1000 counts per second.

dix A), but this colocalization efficiency was much weaker than that of Cy5-RD-KLA-Gffy. Fluorescence microscopy scanning of the brains of CNS-ALL mice showed that the red fluorescence of Cy5-RD-KLA-Gffy and the green fluorescence of Nalm6-luc-EGFP were highly colocalized in the meninges (Fig. 5(c)). IHC confirmed the overexpression of integrin α6 within the CNS-ALL lesions (Fig. 5(d)). Taken together, the results in the Nalm6-luc-EGFP subcutaneous tumor mouse model and the meningeal metastatic tumor mouse model further verified the specific targeting ability of the self-assembling nanopeptide RD-KLA-Gffy to leukemia cells, indicating ideal applicability to CNS-ALL targeted therapy.

3.6. Therapeutic effect of the nanopeptide RD-KLA-Gffy in CNS-ALL mice

Generally, peptide drugs show good biocompatibility, few adverse reactions, and low biological toxicity [40,41]. Toxicity analysis *in vivo* was performed during RD-KLA-Gffy treatment. The data showed that RD-KLA-Gffy treatment did not cause significant changes in body weight (Fig. S13(a) in Appendix A), and the blood biochemical indices also remained within a normal range (Table S3 in Appendix A). In addition, there were no obvious pathological lesions in the main organs, indicating that systemic side effects during RD-KLA-Gffy treatment were rare (Fig. S13(b) in Appendix A).

To explore the biological and therapeutic significance of RD-KLA-Gffy *in vivo*, we examined the survival of Nalm6-luc-EGFP tumor-burdened mice that received RD-KLA-Gffy and peptide control treatment (Fig. 6(a)). After twenty days of administration, the body weights of mice in the saline and KLA-Gffy groups decreased because of disease progression. Conversely, the body weight of mice in the RD-KLA-Gffy treatment group remained normal, suggesting that RD-KLA-Gffy suppressed disease progression (Fig. 6(b)). IVIS imaging also showed that the luminescence signal of

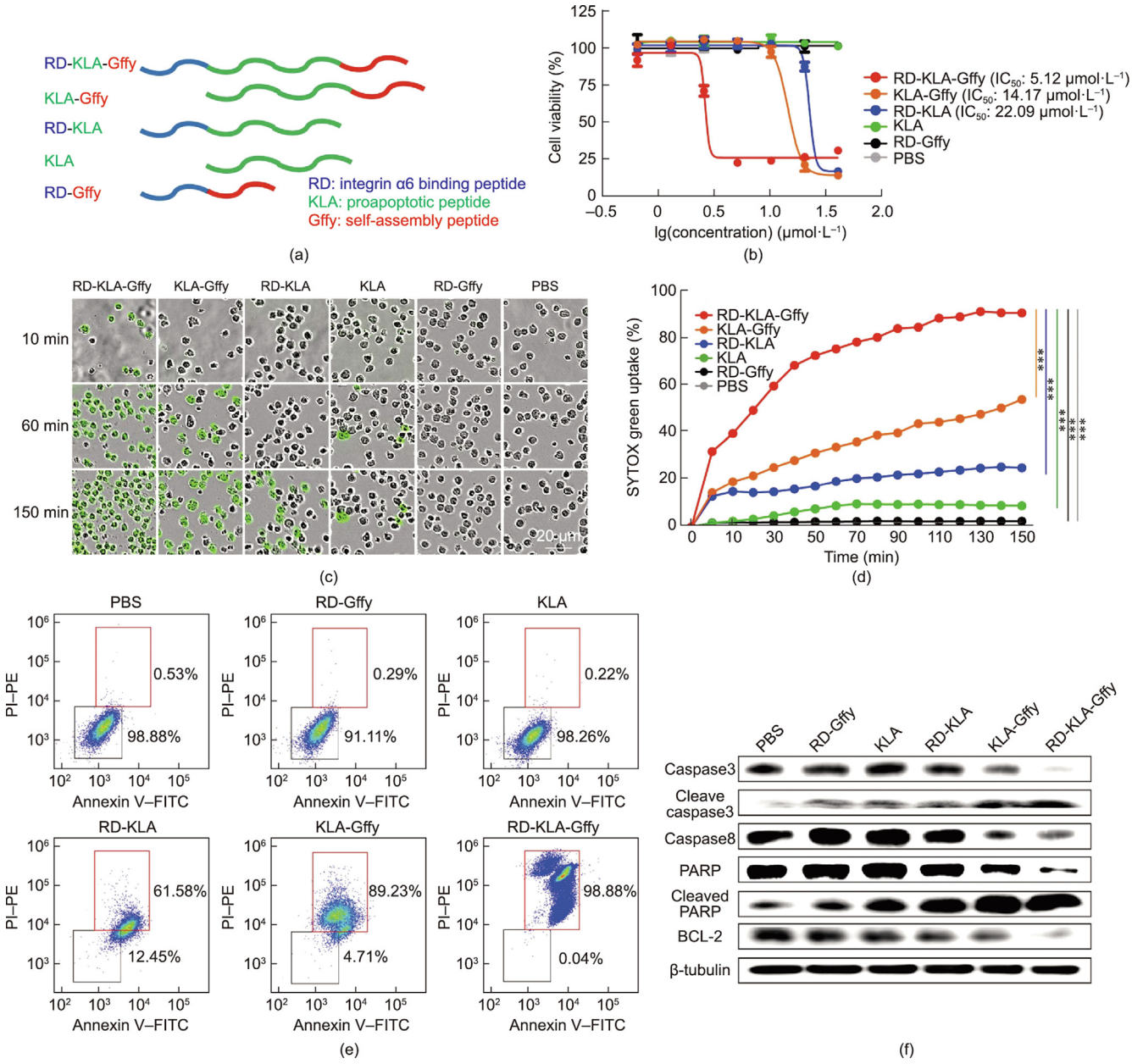

Fig. 4. Proapoptotic effect of the integrin α6-targeted self-assembling nanopeptide RD-KLA-Gffy. (a) Schematic diagram of the nanopeptide RD-KLA-Gffy and other partial dysfunctional control peptides. (b) IC_{50} values of RD-KLA-Gffy and control peptides against Nalm6 leukemia cells. (c) RD-KLA-Gffy and control peptides induced cytotoxicity in Nalm6 cells, as measured using SYTOX green. Fluorescence microscopy images of Nalm6 cells treated with 5 μmol·L^{-1} peptides. (d) Time course plot of dead cells measured using SYTOX green with the operetta cell imaging system. Significance was determined by two-way ANOVA, ***$P < 0.001$. (e) Flow cytometry analysis of annexin V–FITC and propidium iodide (PI)-stained Nalm6 cells treated with 5 μmol·L^{-1} peptides. (f) Western blot analysis of the proapoptotic mechanism in Nalm6 cells.

Nalm6-luc-EGFP in the RD-KLA-Gffy group was significantly lower than that in the control groups on the twentieth day of administration (Figs. 6(c) and (d); Fig. S14 in Appendix A). In addition, the median survival of the mice in the saline, RD-KLA, KLA-Gffy, and RD-KLA-Gffy groups was 14, 17, 19, and 22 d, respectively, indicating that the nanopeptide RD-KLA-Gffy effectively prolonged the survival of CNS-ALL mice (Fig. 6(e)). To further verify the therapeutic use of RD-KLA-Gffy, we treated mice with a combination of RD-KLA-Gffy and MTX. NIRF imaging showed that Nalm6-luc-EGFP metastasis was significantly suppressed in the combination group compared with the RD-KLA-Gffy and MTX groups (Fig. 6(f)). In addition, the median survival of the mice in the saline, RD-KLA-Gffy, MTX, and RD-KLA-Gffy + MTX groups was 17, 22, 21, and 30 d, respectively (Fig. 6(g)). Taken together, these data obtained in CNS-ALL mice demonstrated that RD-KLA-Gffy had promise for therapeutic application as a single agent or in combination with MTX.

3.7. Sketch map

This study identified the high-affinity integrin α6-targeting peptides RWYD and RD through alanine scanning, truncation, molecular docking, and D-substitution. Based on the peptide, we designed an antileukemia self-assembled nanopeptide RD-KLA-Gffy and verified the specificity of this nanopeptide for CNS-ALL lesions. Our data demonstrated that RD-KLA-Gffy has a potent antileukemia effect through inducing cancer cell apoptosis, and

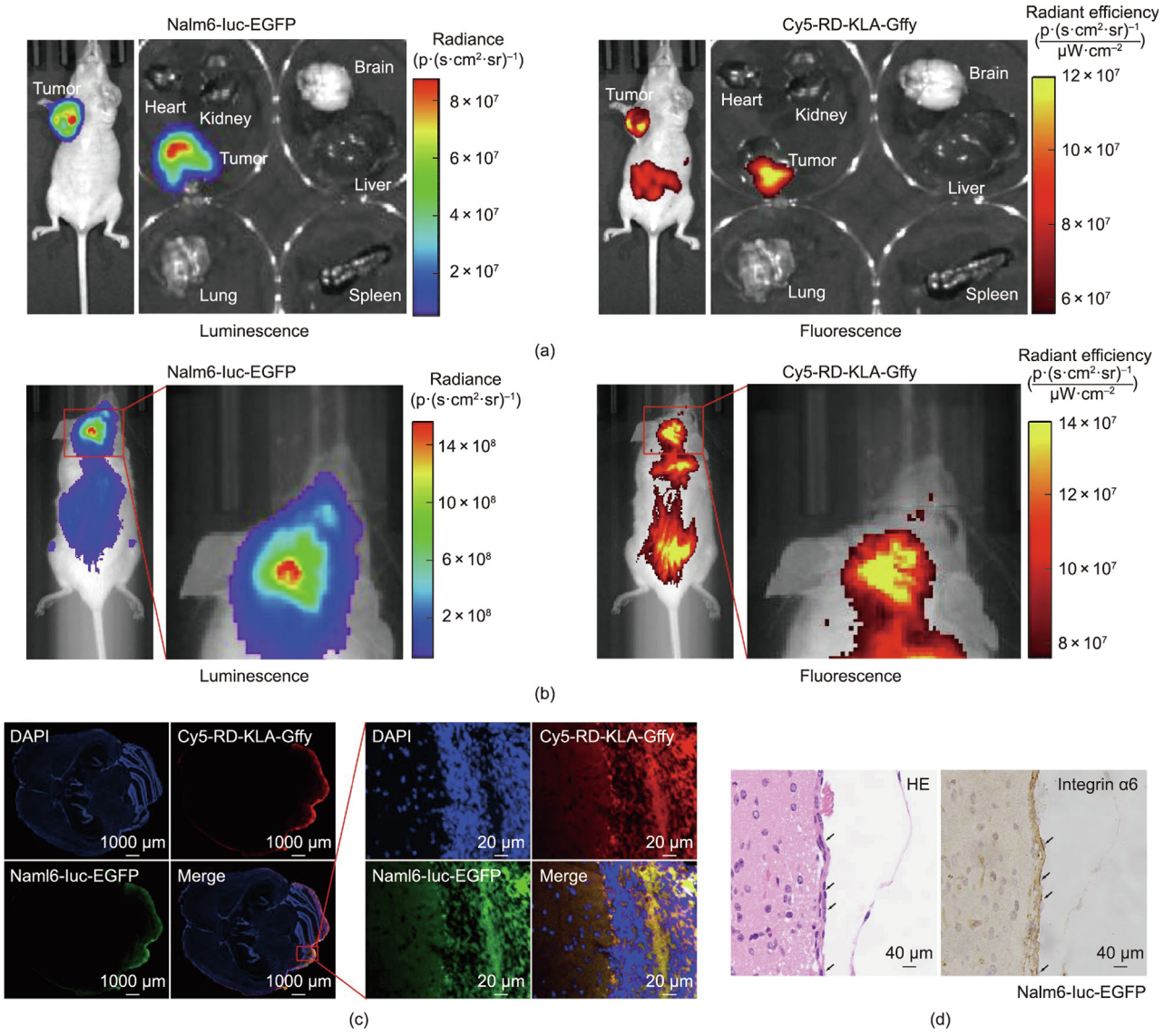

Fig. 5. Tumor uptake of the integrin α6-targeted self-assembling nanopeptide RD-KLA-Gffy. (a,b) *In vivo* imaging of Nalm6-luc-EGFP subcutaneous mice and CNS-ALL mice after treatment with Cy5-RD-KLA-Gffy for 48 h, showing the colocalization of luminescence and fluorescence. (c) Confocal microscopy confirmed the colocalization of Nalm6-luc-EGFP cells and Cy5-RD-KLA-Gffy in the brain parenchymal tissues of CNS-ALL mice. (d) HE staining (left) confirmed the presence of Nalm6-luc-EGFP cells in the meninges, and IHC (right) confirmed integrin α6 overexpression in the lesion. p: photons; sr: steradian.

the survival of CNS-ALL mice could be significantly prolonged by treatment with RD-KLA-Gffy (Fig. 7).

4. Discussion

Integrin α6 plays an important role in leukemia. As determined from gene expression profiling studies of children with B-ALL, integrin α6 is commonly overexpressed in B-ALL and represents a potentially useful marker for the immunophenotypic detection of MRD [42]. A comprehensive clinical study of integrins in ALL indicated that integrin α6, but not integrin α4, is associated with persistent MRD [43]. Leukemia cells mainly exist in the meninges that cover the brain and spinal cord, and invade the brain parenchyma only in advanced stages. Integrin α6-laminin interactions mediate the migration of ALL cells toward the CSF [26]. Treatment with the PI3K inhibitor GS-649443 or specific α6 integrin-neutralizing antibodies reduced integrin α6 expression in cultured B-ALL cells, reduced CNS involvement and prolonged the survival of B-ALL xenografted animals [26]. The Food and Drug Administration (FDA)-approved pan-PI3K inhibitor copanlisib downregulated B-ALL α6 integrin expression, decreased CNS invasion, inhibited bone marrow (BM) disease progression, and improved the response to chemotherapy in leukemic mice [44]. A phase I clinical trial of copanlisib is currently underway to investigate the effects of integrin α6 expression and lymphocyte proliferation in adult patients with refractory or relapsed B-ALL (NCT04803123). Various other integrins have been linked to CNS-ALL, but no drugs targeting integrins or their downstream signaling pathways have progressed to clinical testing.

In a previous study, we reported the integrin α6-targeted peptides RWY and S5, which were employed for molecular imaging in CNS-ALL mice [32]. Although RWY and S5 already have considerable tumor-targeting effects, both still have relatively low affinities for integrin α6 (micromolar range). To find optimized integrin α6-targeted peptides with enhanced binding affinity for integrin α6, three peptide scanning techniques, alanine scanning, truncation, and D-substitution, were used. Alanine scanning systemically replaces each peptide residue with alanine. Alanine scanning can

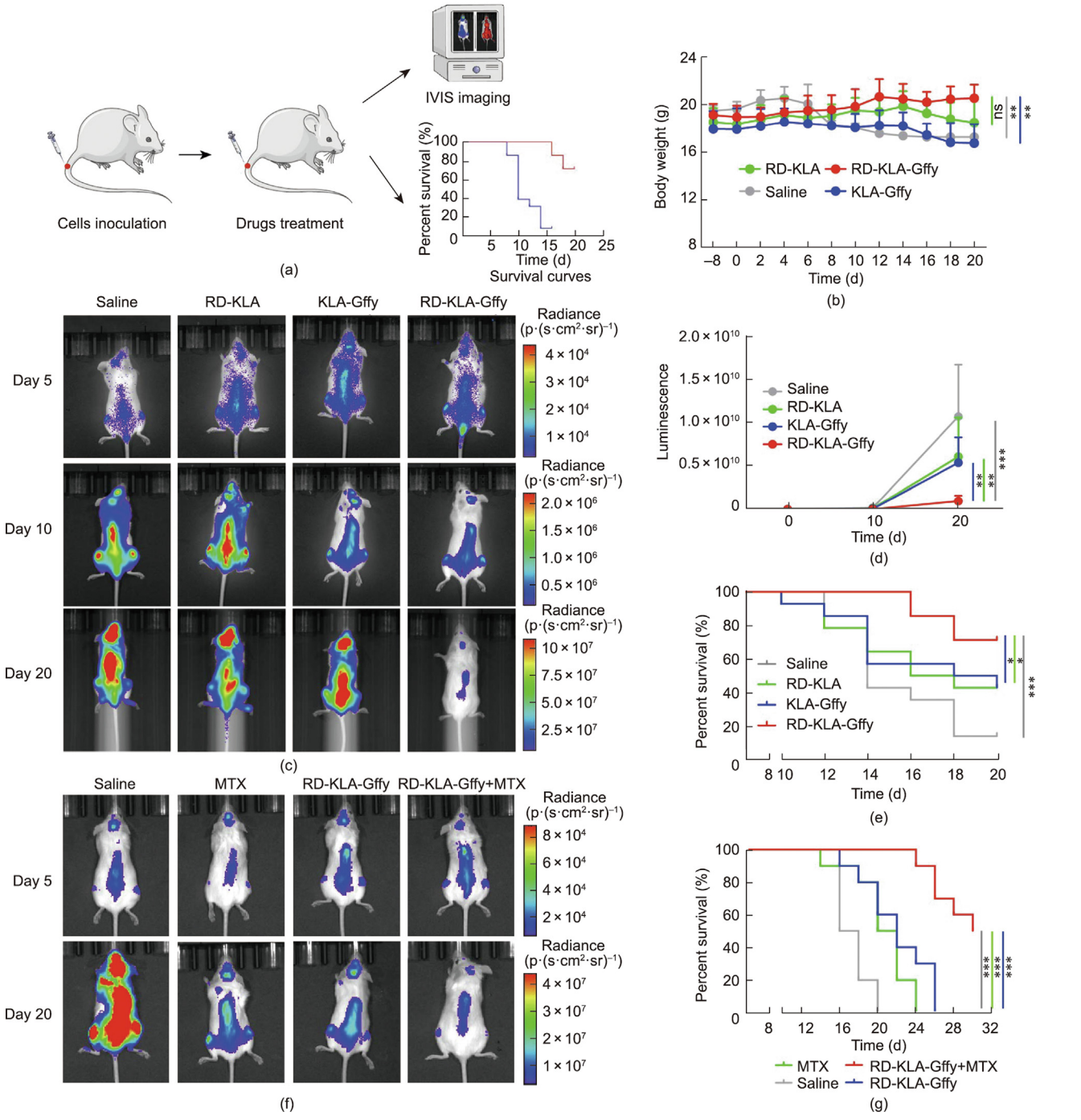

Fig. 6. Therapeutic effect of the integrin α6-targeted self-assembling nanopeptide RD-KLA-Gffy on CNS-ALL. (a) Schematic illustration of the survival experiment. NSG mice were transplanted with Nalm6-luc-EGFP cells. Eight days later, CNS-ALL mice were divided into groups and treated intravenously with drugs every two days. The concentration of RD-KLA-Gffy and control peptides was 5 mg·kg^{-1}. The concentration of MTX was 2 mg·kg^{-1}. The body weights and survival curves of the CNS-ALL mice and Nalm6-luc-EGFP cell metastasis were monitored. (b) Effects of different treatments on the body weight of CNS-ALL mice at the indicated time points. (c) Luminescence images, (d) quantitative analysis of the luminescence signals and (e) survival curves of CNS-ALL mice treated with RD-KLA-Gffy, KLA-Gffy, RD-KLA and saline. (f) Luminescence images and (g) survival curves of CNS-ALL mice treated with RD-KLA-Gffy + MTX, RD-KLA-Gffy, MTX, and saline. Significance was determined by two-way ANOVA ((b) and (d)), n = 6, or log-rank tests ((e) and (g)), n = 10. $^{*}P < 0.05$, $^{**}P < 0.01$, $^{***}P < 0.001$.

determine permissive positions within the sequence for rational optimization because replacement with alanine is expected to have little impact on structure, and to be neutral in structure-activity relationship studies. Alanine scanning has been used extensively, particularly with the cell-permeable peptide TAT-RasGAP317-326 [45], a vasoactive intestinal peptide [46], and sunflower trypsin inhibitor-1 [47]. Furthermore, truncation can identify biologically active peptides with reduced size that can be synthesized at lower cost. Truncation was applied to the antimicrobial peptide anoplin [48], neurokinin-1 receptor tachykinin peptide substance P [49], and secretin receptor analogous peptide [50]. Additionally, D-substitution replaces amino acids with their enantiomers (an L-amino acid is replaced with its corresponding D-amino acid). D-substitution can improve the biostability and efficiency of peptide

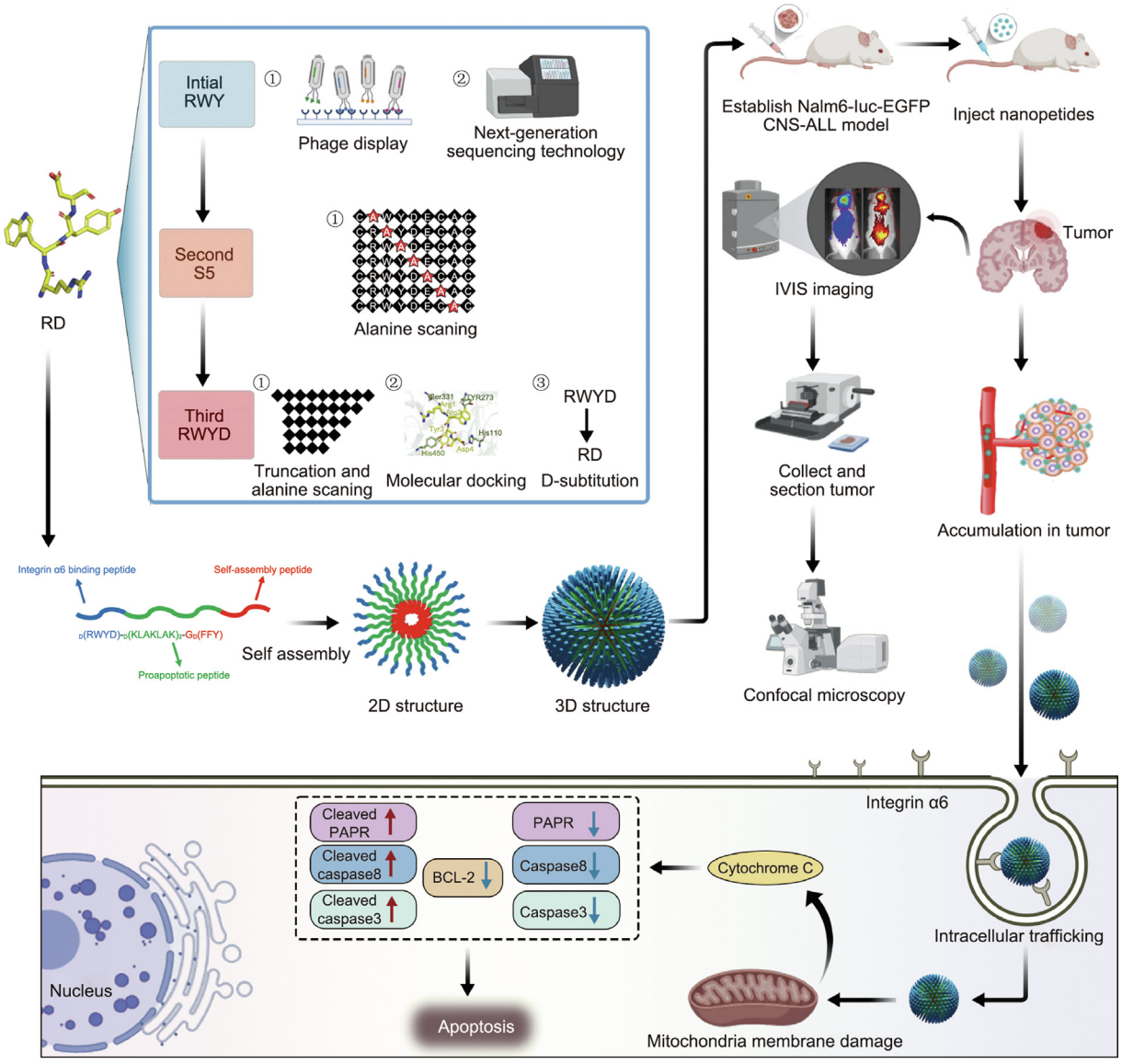

Fig. 7. The sketch map of this study.

drugs. D-substitution was applied with T-cell receptor contact residues [51], the antimicrobial peptide D enantiomer of LL-37 (D-LL-37) [52], and peptide inhibitors of p53-murine double minute 2 and X (p53-MDM2/MDMX) interactions [53]. Therefore, using alanine scanning and truncation techniques, we systemically designed a series of mutant peptides based on RWY and S5, and evaluated their affinities to integrin α6β4 by MST assay (Table 1). Surprisingly, the linear peptide RWYD had nanomolar affinity for integrin α6, an increase of approximately 319-fold compared to that of the peptide RWY ((21.82 ± 3.86) nmol·L^{-1} vs. (6.97 ± 1.44) μmol·L^{-1}). Moreover, we examined the affinities of the peptides for integrin α6 by molecular docking (Fig. 1(c)) and flow cytometry (Fig. 2). Additionally, D-amino acids are usually more stable than L-amino acids; thus, the D-amino acid sequence RD was used for the development of the self-assembling nanopeptide RD-KLA-Gffy.

Anticancer bioactive peptides (ACPs) have potential applications in cancer therapeutics [54,55]. To increase their specificity and reduce their toxicity, ACPs are usually conjugated with tumor-targeting peptides. The proapoptotic peptide KLA is a well-known ACP that was first reported by Ellerby [56]. KLA is nontoxic to normal cells; however, once it is introduced into cancer cells by cell-penetrating peptides (CPPs), it can destroy the mitochondrial membrane, leading to the release of cytochrome C, promoting the cleavage and activation of caspase-3, and ultimately promoting cellular apoptosis. KLA has also been tested for toxicity in mice and appeared nontoxic over a 3-month period [56]. In addition, KLA was conjugated with the well-known integrin αvβ3-targeting peptide RGD to form a tumor-targeting ACP with antitumor effects and low systemic toxicity [56–58]. Conversely, high-dose MTX can cause significant toxicity, especially acute kidney injury (AKI), in 2%–12% of patients [59].

Compared with linear peptides and cyclic peptides, self-assembled peptides have the advantages of good stability, targeted or controlled release, and immune enhancement [60]. It is well-known that linear peptides are less stable than cyclic peptides, and cyclic peptides are more stable but more expensive to synthesize. The peptide self-assembly strategy can fix peptides into a specific shape in a particular environment, and increase the stability of peptides to some extent [61]. It has also been reported that self-assembled peptides can act as adjuvants to enhance both cellular and humoral immunity [62]. The tetrapeptide Gffy is a self-assembling peptide composed of four amino acids in the sequence L-glycine, D-phenylalanine, D-phenylalanine, and D-tyrosine. Gffy can be linked to ACPs to form water-soluble self-assembling

nanoparticles, which can effectively enhance the stability of ACPs, reduce the plasma clearance rate, and promote the internalization of drugs into tumor cells [34]. Gffy has been employed for the treatment of lung and breast cancer [34,63]. Here, we recombined the proapoptotic peptide KLA, the self-assembling peptide Gffy, and the optimized integrin α6-targeted peptide RD to design the self-assembling nanopeptide RD-KLA-Gffy, which showed highly efficient antileukemia activity by inducing apoptosis (Fig. 4). RD-KLA-Gffy was specifically enriched in leukemia lesions (Fig. 5) and prolonged the survival of CNS-ALL mice. Importantly, the combined effect of RD-KLA-Gffy and MTX was superior to their individual therapeutic effects (Fig. 6). Therefore, RD-KLA-Gffy can effectively improve the survival of CNS-ALL mice on the basis of the traditional clinical treatment method (MTX-based chemotherapy).

Based on the marked effect of the nanopeptide RD-KLA-Gffy combined with MTX in the treatment of CNS-ALL, we can directly conjugate RD-KLA-Gffy with MTX through a linker to form a peptide-drug conjugate (PDC), which may simplify the drug administration process and improve the therapeutic effect. Antibody-drug conjugates (ADCs) of MTX have been shown to be effective in the treatment of canine B-cell lymphoma [64]. Compared with ADCs, PDCs have the advantages of smaller molecular weight, stronger tumor penetration, and lower immunogenicity [65], while also crossing the blood–brain barrier into the CNS more easily [66]. Furthermore, we can conjugate RD-KLA-Gffy or RD-Gffy with a 1,4,7,10-tetraazacyclododecane-N,N′,N″,N‴-tetraacetic acid (DOTA) chelator to form radionuclide-drug conjugates (RDCs). These RDCs can be labeled with gallium-68 for the noninvasive detection of CNS-ALL using PET imaging or labeled with lutetium-177 for the treatment of CNS-ALL. We already have considerable experience in the field of RDCs, such as the second integrin α6-targeted peptide S5, which was used for PET imaging in CNS-ALL mice [32], and extra domain B containing fibronectin (EDB FN) targeted probes for surgical navigation, PET imaging, and therapy in thyroid cancer [67]. Therefore, the nanopeptides RD-KLA-Gffy or RD-Gffy have great application prospects as tools for the development of specific payload delivery systems, which might be applied for noninvasive imaging and targeted therapy with low toxicity.

This study has several limitations. First, the *in vivo* experiments were performed with only one cell line, Nalm6. Nalm6 was derived from a patient who suffered CNS disease relapse, and the CNS-ALL mouse model obtained by the introduction of Nalm6 is a reproducible and widely accepted model. Therefore, we used Nalm6 in the initial *in vivo* experiments to verify the therapeutic efficacy of the nanopeptide. However, other cell lines might be less sensitive to caspase-mediated apoptosis; therefore, we should perform mouse experiments with other ALL cell lines, such as RCH-ACV and LAX7R. Second, because lymphoblasts from patients with relapsed ALL can better reflect the clinical therapeutic effect, more experiments need to be performed before the first human trials. Third, our study describes the pathway of RD-KLA-Gffy into cells using integrin α6-mediated internalization, and the enhanced permeability and retention (EPR) effect of nanoparticles, but we have not elucidated how RD-KLA-Gffy is released and degraded. How does it escape from the endosome/lysosome? To address the above questions, we will systematically perform more experiments and report them in our next study.

5. Conclusions

In summary, we optimized a high-affinity integrin α6-targeted peptide RD and further designed an antileukemia self-assembling nanopeptide RD-KLA-Gffy. This nanopeptide induced apoptosis in leukemia cells, specifically enriched in CNS-ALL lesions, and prolonged the survival of CNS-ALL mice when used alone or combined with MTX. Thus, the integrin α6-targeted self-assembling nanopeptide RD-KLA-Gffy has promising applications in the treatment of CNS-ALL.

Acknowledgments

We thank Man-Zhi Li, Bo-Yu Yuan, Jing Wang, and Yong-Jian Peng for their excellent technical assistance. This work has been supported by grants from the National Natural Science Foundation of China (81972531, 82373175, 82102775, and 82002466), the Major Scientific and Technological Projects of Guangdong Province (2019B020202002), and Young Talents Program of Sun Yat-sen University Cancer Center (YTP-SYSUCC-0067). The authenticity of this study has been validated by uploading the key raw data onto the Research Data Deposit (RDD) public platform[‡], with the approval RDD number of RDDB2023462053.

Authors' contribution

Jia-Cong Ye, Wan-Qiong Li, Mei-Ling Chen, and Qian-Kun Shi collected, analyzed, and interpreted the data obtained from all experiments. Hua Wang, Xin-Ling Li, Ying-He Li, Jie Yang, Qiao-Li Wang, and Fang Hu provided resources and assistance. Jia-Cong Ye, Wan-Qiong Li, and Guo-Kai Feng wrote the manuscript. Yan-Feng Gao, Shu-Wen Liu, Mu-Sheng Zeng, and Guo-Kai Feng supervised the experiments and reviewed the manuscript. All the authors have read and approved the final manuscript.

Compliance with ethics guidelines

Jia-Cong Ye, Wan-Qiong Li, Mei-Ling Chen, Qian-Kun Shi, Hua Wang, Xin-Ling Li, Ying-He Li, Jie Yang, Qiao-Li Wang, Fang Hu, Yan-Feng Gao, Shu-Wen Liu, Mu-Sheng Zeng, and Guo-Kai Feng declare that they have no conflict of interest or financial conflicts to disclose.

Appendix A. Supplementary data

Supplementary data to this article can be found online at https://doi.org/10.1016/j.eng.2023.11.012.

References

[1] Krishnan S, Wade R, Moorman AV, Mitchell C, Kinsey SE, Eden TOB, et al. Temporal changes in the incidence and pattern of central nervous system relapses in children with acute lymphoblastic leukaemia treated on four consecutive Medical Research Council trials, 1985–2001. Leukemia 2010;24(2):450–9.
[2] Jeha S, Pei D, Choi J, Cheng C, Sandlund JT, Coustan-Smith E, et al. Improved CNS control of childhood acute lymphoblastic leukemia without cranial irradiation: St Jude Total Therapy Study 16. J Clin Oncol Off J Am Soc Clin Oncol 2019;37(35):3377–91.
[3] Byrnes DM, Vargas F, Dermarkarian C, Kahn R, Kwon D, Hurley J, et al. Complications of intrathecal chemotherapy in adults: single-institution experience in 109 consecutive patients. J Oncol 2019;2019:4047617.
[4] Thastrup M, Duguid A, Mirian C, Schmiegelow K, Halsey C. Central nervous system involvement in childhood acute lymphoblastic leukemia: challenges and solutions. Leukemia 2022;36(12):2751–68.
[5] Veerman AJ, Kamps WA, van den Berg H, van den Berg E, Bökkerink JPM, Bruin MCA, et al. Dexamethasone-based therapy for childhood acute lymphoblastic leukaemia: results of the prospective Dutch Childhood Oncology Group (DCOG) protocol ALL-9 (1997–2004). Lancet Oncol 2009;10(10):957–66.
[6] Iyer NS, Balsamo LM, Bracken MB, Kadan-Lottick NS. Chemotherapy-only treatment effects on long-term neurocognitive functioning in childhood ALL survivors: a review and meta-analysis. Blood 2015;126(3):346–53.
[7] Jacola LM, Krull KR, Pui CH, Pei D, Cheng C, Reddick WE, et al. Longitudinal assessment of neurocognitive outcomes in survivors of childhood acute

‡ www.researchdata.org.cn

lymphoblastic leukemia treated on a contemporary chemotherapy protocol. J Clin Oncol Off J Am Soc Clin Oncol 2016;34(11):1239–47.
[8] Le Jeune C, Thomas X. Potential for bispecific T-cell engagers: role of blinatumomab in acute lymphoblastic leukemia. Drug Des Devel Ther 2016;10:757–65.
[9] Maude SL, Frey N, Shaw PA, Aplenc R, Barrett DM, Bunin NJ, et al. Chimeric antigen receptor T cells for sustained remissions in leukemia. N Engl J Med 2014;371(16):1507–17.
[10] Schewe DM, Alsadeq A, Sattler C, Lenk L, Vogiatzi F, Cario G, et al. An Fc-engineered CD19 antibody eradicates MRD in patient-derived *MLL*-rearranged acute lymphoblastic leukemia xenografts. Blood 2017;130(13):1543–52.
[11] Vogiatzi F, Winterberg D, Lenk L, Buchmann S, Cario G, Schrappe M, et al. Daratumumab eradicates minimal residual disease in a preclinical model of pediatric T-cell acute lymphoblastic leukemia. Blood 2019;134(8):713–6.
[12] Alsadeq A, Lenk L, Vadakumchery A, Cousins A, Vokuhl C, Khadour A, et al. IL7R is associated with CNS infiltration and relapse in pediatric B-cell precursor acute lymphoblastic leukemia. Blood 2018;132(15):1614–7.
[13] Dai H, Zhang W, Li X, Han Q, Guo Y, Zhang Y, et al. Tolerance and efficacy of autologous or donor-derived T cells expressing CD19 chimeric antigen receptors in adult B-ALL with extramedullary leukemia. Oncoimmunology 2015;4(11):e1027469.
[14] Jacoby E, Ghorashian S, Vormoor B, de Moerloose B, Bodmer N, Molostova O, et al. CD19 CAR T-cells for pediatric relapsed acute lymphoblastic leukemia with active CNS involvement: a retrospective international study. Leukemia 2022;36(6):1525–32.
[15] Tasian SK, Gardner RA. CD19-redirected chimeric antigen receptor-modified T cells: a promising immunotherapy for children and adults with B-cell acute lymphoblastic leukemia (ALL). Ther Adv Hematol 2015;6(5):228–41.
[16] De Franceschi N, Hamidi H, Alanko J, Sahgal P, Ivaska J. Integrin traffic—the update. J Cell Sci 2015;128(5):839–52.
[17] Krebsbach PH, Villa-Diaz LG. The role of integrin α6 (CD49f) in stem cells: more than a conserved biomarker. Stem Cells Dev 2017;26(15):1090–9.
[18] Gahmberg CG, Grönholm M, Madhavan S, Jahan F, Mikkola E, Viazmina L, et al. Regulation of cell adhesion: a collaborative effort of integrins, their ligands, cytoplasmic actors, and phosphorylation. Q Rev Biophys 2019;52:e10.
[19] Lipscomb EA, Simpson KJ, Lyle SR, Ring JE, Dugan AS, Mercurio AM. The alpha6beta4 integrin maintains the survival of human breast carcinoma cells *in vivo*. Cancer Res 2005;65(23):10970–6.
[20] Skubitz AP, Bast Jr RC, Wayner EA, Letourneau PC, Wilke MS. Expression of alpha 6 and beta 4 integrins in serous ovarian carcinoma correlates with expression of the basement membrane protein laminin. Am J Pathol 1996;148 (5):1445–61.
[21] Yamakawa N, Kaneda K, Saito Y, Ichihara E, Morishita K. The increased expression of integrin α6 (ITGA6) enhances drug resistance in EVI1(high) leukemia. PLoS One 2012;7(1):e30706.
[22] Lathia JD, Gallagher J, Heddleston JM, Wang J, Eyler CE, Macswords J, et al. Integrin alpha 6 regulates glioblastoma stem cells. Cell Stem Cell 2010;6 (5):421–32.
[23] Cruz-Monserrate Z, Qiu S, Evers BM, O'Connor KL. Upregulation and redistribution of integrin alpha6beta4 expression occurs at an early stage in pancreatic adenocarcinoma progression. Mod Pathol an Off J U S Can Acad Pathol Inc 2007;20(6):656–67.
[24] Chen M, Sinha M, Luxon BA, Bresnick AR, O'Connor KL. Integrin alpha6beta4 controls the expression of genes associated with cell motility, invasion, and metastasis, including S100A4/metastasin. J Biol Chem 2008;284(3):1484–94.
[25] Gang EJ, Kim HN, Hsieh YT, Ruan Y, Ogana HA, Lee S, et al. Integrin α6 mediates the drug resistance of acute lymphoblastic B-cell leukemia. Blood 2020;136 (2):210–23.
[26] Yao H, Price TT, Cantelli G, Ngo B, Warner MJ, Olivere L, et al. Leukaemia hijacks a neural mechanism to invade the central nervous system. Nature 2018;560(7716):55–60.
[27] Feng GK, Zhang MQ, Wang HX, Cai J, Chen SP, Wang Q, et al. Identification of an integrin α6-targeted peptide for nasopharyngeal carcinoma-specific nanotherapeutics. Adv Ther 2019;2(7):1900018.
[28] Feng GK, Ye JC, Zhang WG, Mei Y, Zhou C, Xiao YT, et al. Integrin α6 targeted positron emission tomography imaging of hepatocellular carcinoma in mouse models. J Controlled Release Off J Controlled Release Soc 2019;310:11–21.
[29] Xiao YT, Zhou C, Ye JC, Yang XC, Li ZJ, Zheng XB, et al. Integrin α6-targeted positron emission tomography imaging of colorectal cancer. ACS Omega 2019;4(13):15560–6.
[30] Gao S, Jia B, Feng G, Dong C, Du H, Bai L, et al. First-in-human pilot study of an integrin α6-targeted radiotracer for SPECT imaging of breast cancer. Signal Transduction Target Ther 2020;5(1):147.
[31] Mei Y, Li YH, Yang XC, Zhou C, Li ZJ, Zheng XB, et al. An optimized integrin α6-targeted peptide for positron emission tomography/magnetic resonance imaging of pancreatic cancer and its precancerous lesion. Clin Transl Med 2020;10(4):e157.
[32] Zhang W, Li Y, Chen G, Yang X, Hu J, Zhang X, et al. Integrin α6-targeted molecular imaging of central nervous system leukemia in mice. Front Bioeng Biotechnol 2022;10:812277.
[33] Jaber S, Iliev I, Angelova T, Nemska V, Sulikovska I, Naydenova E, et al. Synthesis, antitumor and antibacterial studies of new shortened analogues of $(KLAKLAK)_2$-NH_2 and their conjugates containing unnatural amino acids. Molecules 2021;26(4):898.
[34] Li X, Wang Y, Zhang Y, Liang C, Zhang Z, Chen Y, et al. A supramolecular "trident" for cancer immunotherapy. Adv Funct Mater 2021;31(23):2100729.
[35] Waterhouse A, Bertoni M, Bienert S, Studer G, Tauriello G, Gumienny R, et al. SWISS-MODEL: homology modelling of protein structures and complexes. Nucleic Acids Res 2018;46(W1):W296–303.
[36] Kaur H, Garg A, Raghava GP. PEPstr: a *de novo* method for tertiary structure prediction of small bioactive peptides. Protein Pept Lett 2007;14(7):626–31.
[37] Singh S, Singh H, Tuknait A, Chaudhary K, Singh B, Kumaran S, et al. PEPstrMOD: structure prediction of peptides containing natural, non-natural and modified residues. Biol Direct 2015;10:73.
[38] Pierce BG, Wiehe K, Hwang H, Kim BH, Vreven T, Weng Z. ZDOCK server: interactive docking prediction of protein-protein complexes and symmetric multimers. Bioinformatics 2014;30(12):1771–3.
[39] Li W, Zhu X, Zhou X, Wang X, Zhai W, Li B, et al. An orally available PD-1/PD-L1 blocking peptide OPBP-1-loaded trimethyl chitosan hydrogel for cancer immunotherapy. J Controlled Release Off J Controlled Release Soc 2021;334:376–88.
[40] Tesauro D, Accardo A, Diaferia C, Milano V, Guillon J, Ronga L, et al. Peptide-based drug-delivery systems in biotechnological applications: recent advances and perspectives. Molecules 2019;24(2):E351.
[41] Lau JL, Dunn MK. Therapeutic peptides: historical perspectives, current development trends, and future directions. Bioorg Med Chem 2017;26 (10):2700–7.
[42] DiGiuseppe JA, Fuller SG, Borowitz MJ. Overexpression of CD49f in precursor B-cell acute lymphoblastic leukemia: potential usefulness in minimal residual disease detection. Cytometry Part B 2009;76(2):150–5.
[43] Shah Scharff BFS, Modvig S, Thastrup M, Levinsen M, Degn M, Ryder LP, et al. A comprehensive clinical study of integrins in acute lymphoblastic leukemia indicates a role of α6/CD49f in persistent minimal residual disease and α5 in the colonization of cerebrospinal fluid. Leuk Lymphoma 2020;61(7):1714–8.
[44] Ridge SM, Whiteley AE, Yao H, Price TT, Brockman ML, Murray AS, et al. Pan-PI3Ki targets multiple B-ALL microenvironment interactions that fuel systemic and CNS relapse. Leuk Lymphoma 2021;62(11):2690–702.
[45] Barras D, Chevalier N, Zoete V, Dempsey R, Lapouge K, Olayioye MA, et al. A WXW motif is required for the anticancer activity of the TAT-RasGAP317-326 peptide. J Biol Chem 2014;289(34):23701–11.
[46] Nicole P, Lins L, Rouyer-Fessard C, Drouot C, Fulcrand P, Thomas A, et al. Identification of key residues for interaction of vasoactive intestinal peptide with human VPAC1 and VPAC2 receptors and development of a highly selective VPAC1 receptor agonist. Alanine scanning and molecular modeling of the peptide. J Biol Chem 2000;275(31):24003–12.
[47] Daly NL, Chen YK, Foley FM, Bansal PS, Bharathi R, Clark RJ, et al. The absolute structural requirement for a proline in the P3'-position of Bowman-Birk protease inhibitors is surmounted in the minimized SFTI-1 scaffold. J Biol Chem 2006;281(33):23668–75.
[48] Jin MW, Xu SM, An Q. Central nervous disease in pediatric patients during acute lymphoblastic leukemia (ALL): a review. Eur Rev Med Pharmacol Sci 2018;22(18):6015–9.
[49] Spitsin S, Pappa V, Douglas SD. Truncation of neurokinin-1 receptor-negative regulation of substance P signaling. J Leukocyte Biol 2018;103(6):1043–51.
[50] Salas RL, Garcia JKDL, Miranda ACR, Rivera WL, Nellas RB, Sabido PMG. Effects of truncation of the peptide chain on the secondary structure and bioactivities of palmitoylated anoplin. Peptides 2018;104:7–14.
[51] Zhang M, Wang Y, Li X, Meng G, Chen X, Wang L, et al. A single L/D-substitution at Q4 of the $mInsA_{2-10}$ epitope prevents type 1 diabetes in humanized NOD mice. Front Immunol 2021;12:713276.
[52] Kim EY, Rajasekaran G, Shin SY. LL-37-derived short antimicrobial peptide KR-12-a5 and its d-amino acid substituted analogs with cell selectivity, anti-biofilm activity, synergistic effect with conventional antibiotics, and anti-inflammatory activity. Eur J Med Chem 2017;136:428–41.
[53] Li X, Liu C, Chen S, Hu H, Su J, Zou Y. D-amino acid mutation of PMI as potent dual peptide inhibitors of p53-MDM2/MDMX interactions. Bioorg Med Chem Lett 2017;27(20):4678–81.
[54] Bakare OO, Gokul A, Wu R, Niekerk LA, Klein A, Keyster M. Biomedical relevance of novel anticancer peptides in the sensitive treatment of cancer. Biomolecules 2021;11(8):1120.
[55] Ghaly G, Tallima H, Dabbish E, Badr ElDin N, Abd El-Rahman MK, Ibrahim MAA, et al. Anti-cancer peptides: status and future prospects. Molecules 2023;28 (3):1148.
[56] Ellerby HM, Arap W, Ellerby LM, Kain R, Andrusiak R, Rio GD, et al. Anti-cancer activity of targeted pro-apoptotic peptides. Nat Med 1999;5(9):1032–8.
[57] Smolarczyk R, Cichoń T, Graja K, Hucz J, Sochanik A, Szala S. Antitumor effect of RGD-4C-GG-$_D$(KLAKLAK)$_2$ peptide in mouse B16(F10) melanoma model. Acta Biochim Pol 2006;53(4):801–5.
[58] Dufort S, Sancey L, Hurbin A, Foillard S, Boturyn D, Dumy P, et al. Targeted delivery of a proapoptotic peptide to tumors *in vivo*. J Drug Targeting 2010;19 (7):582–8.
[59] Howard SC, McCormick J, Pui CH, Buddington RK, Harvey RD. Preventing and managing toxicities of high-dose methotrexate. Oncologist 2016;21 (12):1471–82.
[60] Qi GB, Gao YJ, Wang L, Wang H. Self-assembled peptide-based nanomaterials for biomedical imaging and therapy. Adv Mater 2018;30(22):e1703444.
[61] Zhou Y, Li Q, Wu Y, Li X, Zhou Y, Wang Z, et al. Molecularly stimuli-responsive self-assembled peptide nanoparticles for targeted imaging and therapy. ACS Nano 2023;17(9):8004–25.
[62] Yu X, Zhang Z, Yu J, Chen H, Li X. Self-assembly of a ibuprofen-peptide conjugate to suppress ocular inflammation. Nanomedicine 2017;14 (1):185–93.

[63] Feng K, Ma C, Liu Y, Yang X, Yang Z, Chen Y, et al. Encapsulation of LXR ligand by D-Nap-GFFY hydrogel enhances anti-tumorigenic actions of LXR and removes LXR-induced lipogenesis. Theranostics 2021;11 (6):2634–54.
[64] Lisowska M, Milczarek M, Ciekot J, Kutkowska J, Hildebrand W, Rapak A, et al. An antibody specific for the dog leukocyte antigen DR (DLA-DR) and its novel methotrexate conjugate inhibit the growth of canine B cell lymphoma. Cancers 2019;11(10):E1438.
[65] Zhu YS, Tang K, Lv J. Peptide-drug conjugate-based novel molecular drug delivery system in cancer. Trends Pharmacol Sci 2021;42(10):857–69.
[66] Zhou X, Smith QR, Liu X. Brain penetrating peptides and peptide-drug conjugates to overcome the blood-brain barrier and target CNS diseases. Wiley Interdiscip Rev Nanomed Nanobiotechnol 2021;13(4):e1695.
[67] Li R, He H, Li X, Zheng X, Li Z, Zhang H, et al. EDB-FN targeted probes for the surgical navigation, radionuclide imaging, and therapy of thyroid cancer. Eur J Nucl Med Mol Imaging 2023;50(7):2100–13.